Spin vector alignment of Koronis family asteroids

Stephen M. Slivan

Department of Earth, Atmospheric, and Planetary Sciences, Massachusetts Institute of Technology, 77 Massachusetts Avenue, Rm 54-410, Cambridge, Massachusetts 02139, USA

Studies of asteroid families—groups of asteroids that formed from the fragmentation of larger bodies—are of broad interest to solar system researchers because they can provide insights into collisional processes, as well as the interior structures, strengths, and compositions of asteroids. It is generally accepted that members of the Koronis family were created by collisional disruption of a homogeneous parent body[1] and therefore share the same formation age and subsequent collisional history. The temporal variations in observed brightnesses of the Koronis family members (a consequence of their rotation) are, however, larger than expected[2]. Preferential alignment of spin vectors had been proposed[2] as a possible explanation, but recent modelling[3] predicted that family formation yields random spin vectors among the resulting fragments. Both hypotheses have been untested by observations. Here I show that the actual distribution of spin vectors among the largest members of the Koronis family falls within markedly nonrandom 'spin clusters'. Reconciling models of family formation and evolution with the unexpected alignments of spin obliquities and correlations with spin rates presents a new challenge in understanding asteroid collisional processes.

Over 200 members of the Koronis family of asteroids have been identified[4] among the thousands of objects in the main belt between Mars and Jupiter. Even the largest members of this family are too small directly to observe their shapes and orientations from Earth; instead, their spin states must be inferred from rotation light curves (Fig. 1). A substantial amount of observational data is needed to disentangle the spin vector information from the effects of shape and changing illumination geometry (Fig. 2). I used over 200 light curves spanning 46 yr (Table 1) to derive the spin vectors for nine of the largest members of the Koronis family. Most of the data were obtained between 1983 and 2001 during a series of observing programs that specifically targeted Koronis family asteroids[5–8].

Four different and independent methods of pole determination were used together to derive the spin vectors of the Koronis family sample objects. Two of the methods, weighted amplitude–aspect (WAA)[9] and simultaneous amplitude–magnitude–aspect (SAM)[9], are amplitude–magnitude methods which model an asteroid as a uniformly bright, featureless, smooth triaxial ellipsoid stably rotating about its shortest axis. WAA makes use of the dependence of amplitude on viewing aspect; SAM models both amplitudes and overall brightnesses. To the extent that an asteroid is well represented by the model, the two methods yield the orientation of the rotation axis, the axial ratios of the model ellipsoid, and the dependence of amplitude and magnitude on solar phase angle.

Amplitude–magnitude methods by themselves cannot distinguish between prograde and retrograde rotation because light curve amplitudes and magnitudes are unaffected by the sense of spin of the object. Epoch methods of pole determination complement amplitude–magnitude results by deducing the sense of spin and sidereal rotation period along with the spin axis orientation from small pole-dependent shifts in the observed times of light curve features. The epoch method that I used, sidereal photometric astrometry (SPA)[9], assumes only that the chosen repeating 'standard feature' of the light curve corresponds to a fixed longitude on the asteroid.

The light curve data were also analysed using a convex polyhedron inversion approach[10,11]. This method models the asteroid as a polyhedron with triangular faces, and unlike the amplitude–magnitude and epoch methods, it compares the corresponding model light curves with observed data points at all available rotational phases. It yields a model shape closely related to the convex hull of the body, as well as the sidereal rotation period, the sense of spin, and the orientation of the rotation pole.

The adopted pole solution for each object is the mean of its pole results from the separate methods, weighted by their estimated individual uncertainties. The overall estimated uncertainties for most of the pole solutions are about ten degrees of arc; the pole latitudes by themselves have estimated uncertainties of about five degrees. A detailed description of the different methods' pole solutions for each object, including the individual results and errors, will be presented in a longer paper[8].

Independent knowledge of the true pole of Koronis family member (243) Ida, determined from the Galileo spacecraft fly-by, was used to validate the analysis techniques. Ida's sidereal period and a spin vector prediction had been determined from ground-based observations and accepted for publication before the encoun-

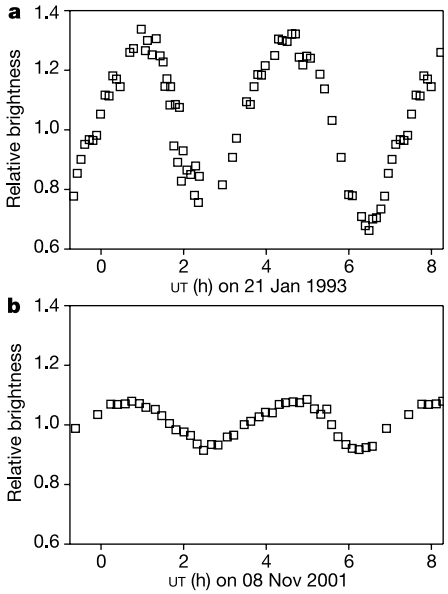

Figure 1 Light curves of (311) Claudia showing the doubly periodic change in brightness as it rotates once in 7.531 h. The brightness variations exhibited by a non-spheroidal asteroid as it rotates are caused mostly by the changes in the illuminated cross-sectional area presented to the observer. The amplitude of the resulting light curve thus depends upon both the object's shape and the angle between the spin axis and the line of sight to the observer. Light curve observations at several different viewing geometries (**a**, **b**) are needed to determine an object's spin vector direction. Koronis family asteroids have been observed specifically for spin vector determination since 1987 at five different observatories using 11 different telescope/detector combinations[6–8]. Nearly 75% of these observations were made using the 0.61-m telescope at the George R. Wallace, Jr Astrophysical Observatory in Westford, Massachusetts, where a 384 × 576-pixel charge-coupled device (CCD) detector was used at Cassegrain focus with 5:1 focal length reduction for an image scale of 2.4 arcsec per pixel and a field size of 15′ × 23′. Integrations were usually 5 min using a *V* filter, and the telescope tracked unguided at the sidereal rate. The full-width at half-maximum of stellar images was typically 5–6″, and the synthetic aperture radius used for photometry was typically 12″. Asteroid brightnesses were measured relative to on-chip comparison stars used as secondary standards. On-chip stars of similar brightness to the asteroid were used to estimate the measurement uncertainties. All objects of interest were measured using the same aperture and sky annulus sizes. Relative brightnesses of comparison stars in different fields close together in the sky were measured within an hour or two of stable sky conditions on clear nights by imaging them rapidly enough to minimize differences in air mass and in time. UT, universal time.

Table 1 **Summary of light curve observations for spin vector analysis**

Object	Years observed	Apparitions	Nights	Observations
(158)	1984–1999	7	37	934
(167)	1977–1993	5	16	334
(208)	1985–1994	5	16	296
(277)	1983–2000	5	27	576
(311)	1984–2001	6	23	580
(321)	1955–2001	8	26	1,054
(534)	1977–1993	6	16	201
(720)	1983–1999	6	36	818
(1223)	1977–1996	7	18	738
Total:		55	215	5,531

An apparition is a period of several months during which the target object can be observed. Apparitions of any particular Koronis family asteroid occur at intervals of about 15 months.

ter[12]; subsequently its pole location was unambiguously derived from resolved images[13]. Applying the same spin vector determination methods used for the Koronis family sample objects to the available light curves of Ida gave a pole solution that is consistent with the true pole, subject to the limitations of the underlying simplifying assumptions made.

A twofold ambiguity is present for each sample object's pole solution: the two equally likely poles for each object have similar ecliptic latitudes and are about 180° apart in ecliptic longitude. It is not possible to identify which of the two solutions is the true pole because the low orbital inclinations of Koronis family members restrict Earth-based viewing geometries to be nearly symmetric with respect to the orbit plane. Nevertheless, the object's spin obliquity (that is, the angle between the spin pole and the orbit pole) can be determined in spite of the pole ambiguity because for low-inclination orbits the obliquity does not strongly depend on the pole longitude. For the Koronis sample objects the obliquities corresponding to each pair of ambiguous poles differ by no more than 3°, and for most of the sample objects the difference is 1° or less, all well within the estimated uncertainties of the derived pole locations.

Including Ida, pole solutions are now available for ten of the largest members of the Koronis family. The histogram of the derived spin vector obliquities shown in Fig. 3a reveals a markedly bimodal distribution. I checked the statistical significance of the distribution using a Kolmogorov–Smirnov test[14], a test for differences between cumulative distributions that is non-parametric (that is, no assumptions are made about the distributions of the populations) and that does not depend on the binning chosen for the data. Applying the test to the values of cos(ε) shows that the distribution differs from a uniform distribution at greater than the 99% confidence level, indicating a statistically significant clustering of the spin vectors in obliquity. The results remain significant at the 95% confidence level even if pole solutions for five more family members were to yield completely random obliquities. Preliminary analysis of the light curve data available through 1994 had suggested the corresponding bimodal distribution in the spin axis latitudes[6], but in the absence of analysis using an epoch method, confidence in the pole latitude results was low and the senses of rotation were unknown.

An unusual anisotropy is apparent in Fig. 3b, where correlation between the spin rates of the sample objects and their obliquities forms two distinct groupings, which I call 'spin clusters'. It is difficult to understand how preferred spin vector obliquities and rotation rates could exist in the context of formation by catastrophic fragmentation and disruption of a parent body, followed by at least 10^9 yr of collisional evolution in the main belt[15]. Current models of

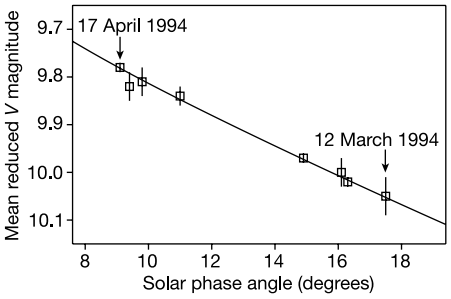

Figure 2 Effect of changing illumination geometry on the observed mean brightness of (158) Koronis during a 36-day interval in 1994. The horizontal axis is the angle between the line of sight and the direction of illumination from the Sun and the vertical axis is brightness, calibrated to standard *V* magnitudes and reduced to unit Earth–asteroid and Sun–asteroid distances. The solid line is the best-fit Lumme–Bowell solar phase function[18]. Solar phase effects must be removed from the calibrated observed light curves to combine data from different apparitions for spin axis determination. To calibrate observations to *V* magnitudes, standard stars[19] with $V \approx 10$–12 and V–R colour ≈ 0.4–0.6 were observed with the comparison stars during photometric conditions. Most of the total uncertainties in the overall transformation to standard *V* are 0.01–0.04 magnitude. Comparison stars used from 1998 to 2001 were calibrated by observing standards with the light curve observations. Comparison stars used from 1992 to 1994 were calibrated during four dedicated observing runs at two mountaintop sites[6,7]. At the Michigan-Dartmouth-MIT Observatory 1.3-m telescope, CCD detectors binned to 512 × 512 pixels were used at Cassegrain focus for image scales of about 1″ per pixel and field sizes about 10′ square. The telescope tracked autoguided at the sidereal rate, and the synthetic aperture radii for photometry were 5–6″. At the McDonald Observatory 0.91-m telescope, CCD detectors binned to about 260 × 260 pixels were used at Cassegrain focus for image scales of about 1″ per pixel and field sizes about 4′ square. The telescope tracked unguided at the sidereal rate, and the synthetic aperture radius was 8″. Integrations were 15–30 s using a *V* filter. Stars that seemed variable or exhibited colour transformation effects were not used as comparison stars.

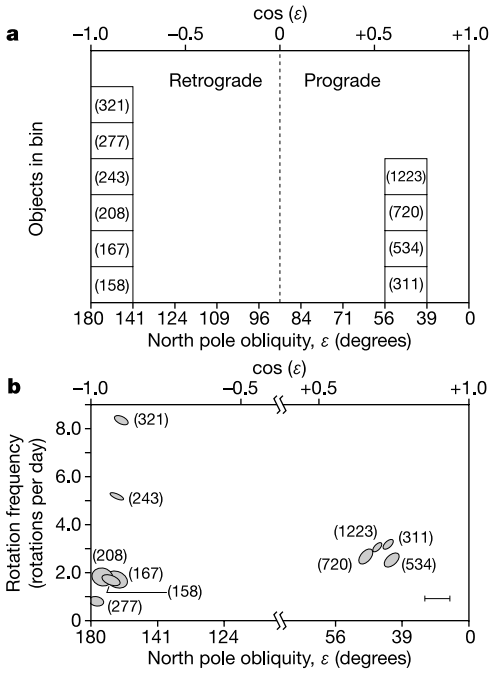

Figure 3 Spin angular momentum in the Koronis family of asteroids. **a**, Distribution of spin vector north pole obliquities ε for the sample objects, whose minor planet numbers are given in parentheses. Poles distributed isotropically on a sphere would give a uniform distribution in cos(ε); the anisotropy of the sample obliquities is significant at greater than the 99% confidence level independent of the binning chosen. **b**, Spin vectors of Koronis family members plotted as rotation frequency versus cos(ε), revealing two 'spin clusters' near (160°,1.7) and (45°,2.9). Each object is represented by an ellipse with size proportional to the object's diameter, axial ratio corresponding to the equatorial view of the object's model shape from its derived pole solution, and that has been rotated counterclockwise by the obliquity. The scale bar at lower right is 50 km. The empty central section of the plot is omitted to save space.

family formation predict that the memory of spin of the original unshattered parent body is lost[3], and existing models of spin angular momentum suggest that collisional evolution randomizes asteroid spin vectors regardless of their initial orientations[2], although the absolute timescale is uncertain. Here, I briefly identify two possible general explanations for future study.

One possibility is that randomly oriented gravitational aggregates from the initial collision have further fragmented, creating smaller objects that have the same spin obliquities as the remnants from which they were formed. Secondary fragmentation of the largest remnant of the initial break-up has previously been proposed to explain the existence of several objects of comparable size among the largest Koronis family members[16], but if the spin clusters were formed in this way then the absence of obvious corresponding associations in proper orbital elements also needs to be explained. To test this hypothesis, further work is needed to better understand the behaviour and evolution of gravitational aggregates.

A second possible explanation for spin clusters is that some dynamical process is aligning the obliquities and matching the rotation rates. Thermal effects can change obliquities and spin rates of small irregular asteroids, but calculations for Ida suggest that asteroids of comparable size are unlikely to have been substantially affected[17]. If a secular effect has clustered the spin vectors, then the present understanding of the timescale over which thermal processes have affected the spin cluster objects may be incomplete, or some nonthermal process may be at work. Finding similar clustering of spins for 20–40-km asteroids outside the Koronis family would support the hypothesis of a secular effect. □

Received 24 May; accepted 18 July 2002; doi:10.1038/nature00993.

1. Chapman, C. R., Paolicchi, P., Zappalà, V., Binzel, R. P. & Bell, J. F. in *Asteroids II* (eds Binzel, R. P., Gehrels, T. & Matthews, M. S.) 386–415 (Univ. Arizona Press, Tucson, 1989).
2. Binzel, R. P. Collisional evolution in the Eos and Koronis asteroid families: Observational and numerical results. *Icarus* **73,** 303–313 (1988).
3. Michel, P., Benz, W., Tanga, P. & Richardson, D. C. Collisions and gravitational reaccumulation: Forming asteroid families and satellites. *Science* **294,** 1696–1700 (2001).
4. Zappalà, V., Bendjoya, Ph., Cellino, A., Farinella, P. & Froeschle, C. Asteroid families: Search of a 12,487-asteroid sample using two different clustering techniques. *Icarus* **116,** 291–314 (1995).
5. Binzel, R. P. A photoelectric survey of 130 asteroids. *Icarus* **72,** 135–208 (1987).
6. Slivan, S. M. *Spin-Axis Alignment of Koronis Family Asteroids* PhD thesis, Massachusetts Institute of Technology (1995).
7. Slivan, S. M. & Binzel, R. P. Forty-eight new rotation lightcurves of 12 Koronis family asteroids. *Icarus* **124,** 452–470 (1996).
8. Slivan, S. M. *et al.* Spin vectors in the Koronis family: Comprehensive results from two independent analyses of 213 rotation lightcurves. *Icarus* (submitted).
9. Drummond, J. D., Weidenschilling, S. J., Chapman, C. R. & Davis, D. R. Photometric geodesy of main-belt asteroids. II. Analysis of lightcurves for poles, periods, and shapes. *Icarus* **76,** 19–77 (1988).
10. Kaasalainen, M. & Torppa, J. Optimization methods for asteroid lightcurve inversion. I. Shape determination. *Icarus* **153,** 24–36 (2001).
11. Kaasalainen, M., Torppa, J. & Muinonen, K. Optimization methods for asteroid lightcurve inversion. II. The complete inverse problem. *Icarus* **153,** 37–51 (2001).
12. Binzel, R. P. *et al.* Asteroid 243 Ida: Ground-based photometry and a pre-Galileo physical model. *Icarus* **105,** 310–325 (1993).
13. Davies, M. E. *et al.* The north pole direction and the control network of the asteroid 243 Ida. *Bull. Am. Astron. Soc.* **26,** 1154–1155 (1994).
14. Miller, I. & Freund, J. E. *Probability and Statistics for Engineers* (Prentice-Hall, Englewood Cliffs, New Jersey, 1977).
15. Belton, M. J. S. *et al.* First images of asteroid 243 Ida. *Science* **265,** 1543–1547 (1994).
16. Marzari, F., Davis, D. & Vanzani, V. Collisional evolution of asteroid families. *Icarus* **113,** 168–187 (1995).
17. Rubincam, D. P. Radiative spin-up and spin-down of small asteroids. *Icarus* **148,** 2–11 (2000).
18. Bowell, E., *et al.* in *Asteroids II* (eds Binzel, R. P., Gehrels, T. & Matthews, M. S.) 524–556 (Univ. Arizona Press, Tucson, 1989).
19. Landolt, A. U. *UVBRI* photometric standard stars around the celestial equator. *Astron. J.* **88,** 439–460 (1983).

Acknowledgements

I thank R. Binzel for advice and encouragement, and M. Kaasalainen, L. Crespo da Silva, M. Lyndaker and M. Krčo for contributions at various stages of this work.

Competing interests statement

The authors declare that they have no competing financial interests.

Correspondence and requests for materials should be addressed to the author (e-mail: slivan@mit.edu).

Collapse and revival of the matter wave field of a Bose–Einstein condensate

Markus Greiner, Olaf Mandel, Theodor W. Hänsch & Immanuel Bloch

Sektion Physik, Ludwig-Maximilians-Universität, Schellingstrasse 4/III, D-80799 Munich, Germany, and Max-Planck-Institut für Quantenoptik, D-85748 Garching, Germany

A Bose–Einstein condensate represents the most 'classical' form of a matter wave, just as an optical laser emits the most classical form of an electromagnetic wave. Nevertheless, the matter wave field has a quantized structure owing to the granularity of the discrete underlying atoms. Although such a field is usually assumed to be intrinsically stable (apart from incoherent loss processes), this is no longer true when the condensate is in a coherent superposition of different atom number states[1–6]. For example, in a Bose–Einstein condensate confined by a three-dimensional optical lattice, each potential well can be prepared in a coherent superposition of different atom number states, with constant relative phases between neighbouring lattice sites. It is then natural to ask how the individual matter wave fields and their relative phases evolve. Here we use such a set-up to investigate these questions experimentally, observing that the matter wave field of the Bose–Einstein condensate undergoes a periodic series of collapses and revivals; this behaviour is directly demonstrated in the dynamical evolution of the multiple matter wave interference pattern. We attribute the oscillations to the quantized structure of the matter wave field and the collisions between individual atoms.

In order to determine the evolution with time of a many-atom state with repulsive interactions in a confining potential, we first assume that all atoms occupy only the ground state of the external potential. The hamiltonian governing the system after subtracting the ground-state energy of the external potential is then solely determined by the interaction energy between the atoms:

$$\hat{H} = \frac{1}{2}U\hat{n}(\hat{n}-1) \qquad (1)$$

Here $\hat{n}$ counts the number of atoms in the confining potential, and U is the on-site interaction matrix element that characterizes the energy cost due to the repulsive interactions when a second atom is added to the potential well. It can be related to the s-wave scattering length a and the ground-state wavefunction $w(\mathbf{x})$ through $U = 4\pi\hbar^2 a/m \int |w(\mathbf{x})|^4 \, \mathrm{d}^3x$, as long as the vibrational level spacing of the external potential is large compared with the interaction energy. The eigenstates of the above hamiltonian are Fock states $|n\rangle$ in the atom number, with eigenenergies $E_n = Un(n-1)/2$. The evolution with time (t) of such an n-particle state is then simply given by $|n\rangle(t) = |n\rangle(0) \times \exp(-iE_n t/\hbar)$, where $\hbar$ is Planck's constant (h) divided by 2π.

We now consider a coherent state $|\alpha\rangle$ (see, for example, ref. 7) of the atomic matter field in a potential well. Such a coherent state with a complex amplitude α and an average number of atoms $\bar{n} = |\alpha|^2$ can be expressed as a superposition of different number states $|n\rangle$ such that $|\alpha\rangle = \exp(-|\alpha|^2/2)\sum_n \frac{\alpha^n}{\sqrt{n!}}|n\rangle$. Now the system is in a superposition of different eigenstates, which evolve in time according to their eigenenergies E_n. This allows us to calculate the evolution with time of an initially coherent state:

$$|\alpha\rangle(t) = \mathrm{e}^{-|\alpha|^2/2}\sum_n \frac{\alpha^n}{\sqrt{n!}}\mathrm{e}^{-i\frac{1}{2}Un(n-1)t/\hbar}|n\rangle \qquad (2)$$

Evaluating the atomic field operator $\hat{a}$ for such a state then yields the